



This is a repository copy of *Detection of onset of agglomeration in a bubbling fluidized bed biomass combustor using reactive Eulerian computational fluid dynamics*.

White Rose Research Online URL for this paper:

<https://eprints.whiterose.ac.uk/216526/>

Version: Accepted Version

Article:

Tasleem, A., Ullah, A. orcid.org/0000-0001-8010-3904, Li, F. et al. (3 more authors) (2024) Detection of onset of agglomeration in a bubbling fluidized bed biomass combustor using reactive Eulerian computational fluid dynamics. *Particuology*, 90. pp. 504-515. ISSN 1674-2001

<https://doi.org/10.1016/j.partic.2023.12.019>

© 2024 The Authors. Except as otherwise noted, this author-accepted version of a journal article published in *Particuology* is made available via the University of Sheffield Research Publications and Copyright Policy under the terms of the Creative Commons Attribution 4.0 International License (CC-BY 4.0), which permits unrestricted use, distribution and reproduction in any medium, provided the original work is properly cited. To view a copy of this licence, visit <http://creativecommons.org/licenses/by/4.0/>

Reuse

This article is distributed under the terms of the Creative Commons Attribution (CC BY) licence. This licence allows you to distribute, remix, tweak, and build upon the work, even commercially, as long as you credit the authors for the original work. More information and the full terms of the licence here:

<https://creativecommons.org/licenses/>

Takedown

If you consider content in White Rose Research Online to be in breach of UK law, please notify us by emailing eprints@whiterose.ac.uk including the URL of the record and the reason for the withdrawal request.



eprints@whiterose.ac.uk
<https://eprints.whiterose.ac.uk/>

Detection of onset of agglomeration in a bubbling fluidized bed biomass combustor using reactive Eulerian computational fluid dynamics

Abdullah Tasleem ^a, Atta Ullah ^{a,*}, Fei Li ^b, Qun Yi ^c, William Nimmo ^d, Syed Sheraz Daood ^{d,f,*}

^a Department of Chemical Engineering, Pakistan Institute of Engineering and Applied Sciences (PIEAS),
Lehtrar Road, P.O. Nilore, 45650, Islamabad, Pakistan

^b Institute of Process Engineering, Chinese Academy of Sciences, Beijing, China

^c School of Chemical Engineering and Pharmacy, Wuhan Institute of Technology, Wuhan, 430205, China

^d Energy Engineering Group, Energy 2050, Department of Mechanical Engineering, University of
Sheffield, Sheffield S3 7RD, United Kingdom

^e Institute of Energy and Environmental Engineering, Faculty of Electrical, Energy & Environmental
Engineering, University of the Punjab, Quaid-e-Azam Campus, Lahore, Pakistan

^f Energy Engineering Research and Development Centre, Faculty of Electrical, Energy & Environmental
Engineering, University of the Punjab, Quaid-e-Azam Campus, Lahore, Pakistan

*Corresponding Authors: E-mail address: atta@pieas.edu.pk (A. Ullah); sdaood.icet@pu.edu.pk (S. Sheraz Daood)

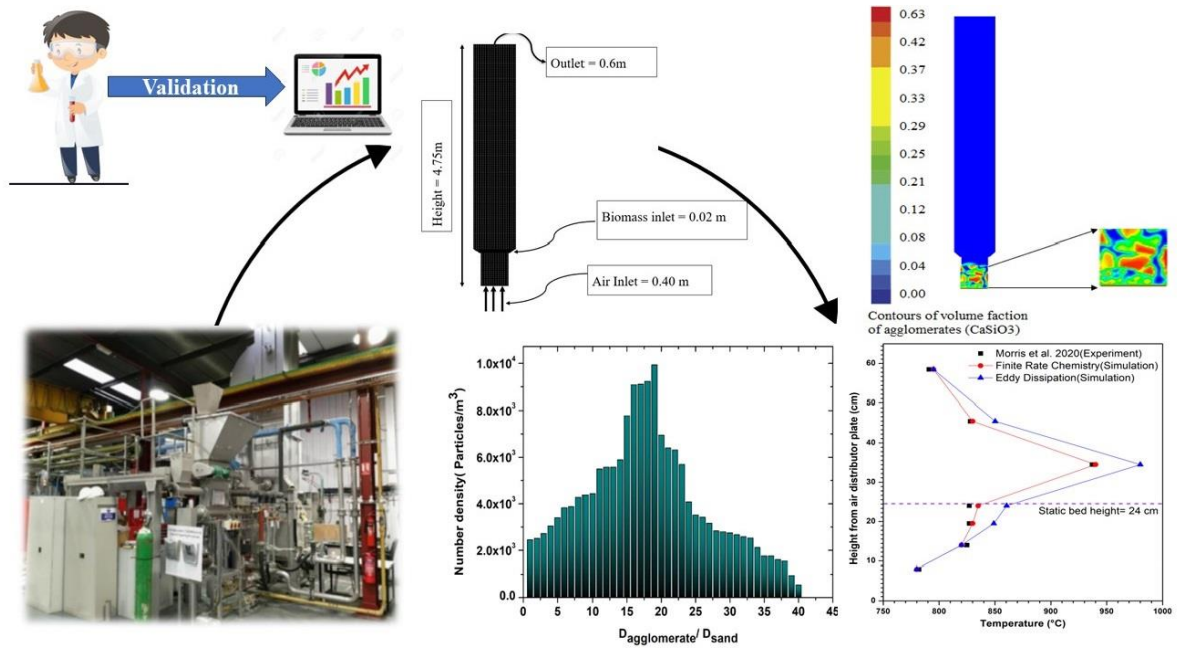
Abstract

The choice of a type of combustion technology to be used for heat or power generation depends on economic, technical, operational and fuel availability constraints. The benefits associated with the evolving market driven by the fluidized bed combustion (FBC) technology cannot be overlooked especially when gauged at 65GW_{th} of worldwide installed capacity alongside added benefits of handling fuel variation, low pollutant emissions and high combustion efficiency. Biomass or biomass waste will continue to have a vital role to play in the future FBC technology-based power generation. Biomass often contains high levels of inorganic species that can form sticky agglomerates posing a significant risk to boiler operation resulting in unscheduled outages. This added complexity of the behaviour of the fuel and bed material mix highlights the requirement for simulation models to identify agglomeration to help improve the overall performance and reliability of FBC technology. To resolve this problem, this research devised a simulation strategy for the detection of agglomeration using the Eulerian–Eulerian approach. The developed modeling strategy is validated with the experimental data available in literature for two-dimensional simplified geometry of a

pilot-scale fluidized bed combustor. The model results were found promising and robust to predict bed defluidization times and other parameters consistent with the experimental data.

Keywords: Fluidized bed combustion; Eulerian; Models; Biomass; Agglomeration; Defluidization

Graphical abstract:



Highlights:

- Innovative FBC combustion & agglomeration modeling.
- PBM-TFM framework predicts FBC agglomeration.
- Validation proves model's real-world applicability.
- Industrial significance: efficient biomass combustion.
- Foundation for future biomass technology.

Nomenclature

FBC	Fluidized Bed Combustor
PBM	Population Balance Model
CFD	Computational Fluid Dynamics
TFM	Two Fluid Model
FVM	Finite Volume Method
KTGF	Kinetic Theory of Granular Flow
PDE	Partial Differential Equation
DEM	Discrete Element Method
ε	Volume fraction
ρ	Density, kg.m ⁻³
U	Instantaneous velocity, m.s ⁻¹
S	Source term
ϕ_{gs}	Drag coefficient between the air and solid phases
\vec{v}	Velocity, m.s ⁻¹
\vec{g}	Gravitational force, m.s ⁻²
$\vec{\tau}$	Stress tensor, Pa
λ_s	Solid bulk viscosity
θ_s	Granular temperature
g_o	Radial distribution function
e	Coefficient of restitution
k	Turbulence kinetic energy
ε	Rate of dissipation
G_k	Generation of turbulence kinetic energy due to mean velocity gradients
G_b	Generation of turbulence kinetic energy due to buoyancy
Y_M	Fluctuating dilatation in compressible turbulence to the overall dissipation rate
σ_k	Turbulent Prandtl numbers for k
σ_ε	Turbulent Prandtl numbers for ε
H	Specific enthalpy
α	Thermal conductivity of mixture
Q	Heat exchange intensity between solid and gas phases
$s_{sg}H_s$	Heat transfer between gas and solid.
H_i	Enthalpy of each specie present in mixture
$R_{s,i}$	Heterogeneous reaction rate
$J_{g,i}$	diffusion flux of species i in gas phase
$R_{g,i}$	net rate of production of homogeneous species i
$B_{ag,i}$	Birth rate due to aggregation
$D_{ag,i}$	Death rate due to aggregation
$B_{br,i}$	Birth rate due to breakage
$D_{br,i}$	Death rate due to breakage
V'	Volume of aggregate particles
$\Omega_{ag}(V_i, V_j)$	Frequency of collisions
$P_{ag}(V_i, V_j)$	Probability that the collision results in coalescence
\bar{u}_{ij}	Characteristic collision of two particles
n_i, n_j	Number densities
We_{ij}	Weber number

Subscripts and Superscripts

g	Gas Phase
s	Solid Phase
i	Species i
b	Buoyancy
M	Fluctuation dilation
k	Turbulence kinetic energy

1. Introduction

Worldwide fluctuations in the price of fuel coupled with strict emission regulations force power generation sectors to burn a diverse range of fuels including biomass under variable load conditions and this led to significant issues with plant efficiency, combustion stability, operation feasibility and emission control. Recent studies demonstrate the potential of fluidized bed biomass combustion for future energy systems from both a techno-economic and an environmental viewpoint. Fluidized bed biomass combustion systems have high flexibility of control, efficient mixing of solids and uniform distribution of heat within the furnace [1]. Besides of many advantages, these systems are still struggling due to different operational problems like corrosion, erosion, slagging, and bed agglomeration which subsequently leads to bed defluidization [2]. One of the significant issues related to the operation of the fluidized bed combustion (FBC) is the formation of agglomerates that is exacerbated due to high ash content present in agricultural leftovers [3]. Agglomeration occurs when particles of bed material stick together to form larger particles, or agglomerates [4]. Agglomerates can lead to several problems, including non-uniform heat distribution and reduced heat transfer rates, increased pressure drop, increased emissions of harmful pollutants. Agglomeration alters the fluidized bed flow regime by lowering mixing quality and defluidizing the bed, resulting in undesirable plant shutdowns [5].

There are a number of ways to reduce agglomeration in fluidized bed combustors (FBCs). The combination of the bed material/additive being one where the transfer of alkali metals in biomass to the additive or minerals would affect the ash fusion temperature of complexes, and thus can control the agglomeration, fouling, slagging, and corrosion formations. An overdose or an inappropriate type of additives can though result in elevated quantities of alkali chlorides leading to chloride-based corrosion in the later sections of the furnace together with non-uniform heat distribution, and tube and wall deposit formations. Some other approaches include using fuels with low ash content, modifying operating conditions, removing alkali metals from the fuel, and using other bed materials [6–8]. Agglomeration is a complicated issue, and no single approach will work for all FBCs. Operators may help to ensure the safe and efficient operation of their FBCs by knowing the elements that lead to agglomeration and the strategies that can be taken to mitigate it [9]. Such strategies involve reducing the operating temperature, boosting gas velocity, and replacing the bed material. However, each choice has substantial drawbacks as well such as lower efficiency, more emissions, or higher costs [10]. Pilot or large-scale plants assist to study the phenomenon of bed agglomeration and its possible counter measures, but these are very expensive and time-consuming process [11–16]. Furthermore, large scale FBC control is inherently multi-variable with high inertia, long delays and strong non-linearity due to its complexity hence computational techniques can be utilized to optimize the operational costs while improving performance of FBCs.

Computational techniques are being increasingly used to study and counter agglomeration in fluidized bed combustors (FBCs). These techniques simulate the flow and behaviour of particles in a fluidized bed, which can help to identify the factors that contribute to agglomeration and to develop strategies for mitigation. Some of the most used computational techniques for studying agglomeration in FBCs include particle tracking methods, which track the motion of individual particles in a fluidized bed [17]. Computational fluid dynamics (CFD) methods can be used to model the flow of fluid and particles in a fluidized bed together with multiphase flow simulations used to study the interactions between different phases of matter, such as gas, liquid, and solid [18]. These computational tools help to investigate agglomeration in FBCs under various situations, including varied fuel types, ash compositions, and operating parameters [19]. This data can then be utilised to develop strategies for preventing agglomeration, using low-ash fuels, adding bed additives, or changing operation settings [20]. The availability of the measurements and simulation data will allow the development of better predictive models for the process control and ultimately the whole combustion process optimisation.

Plant operators can help to ensure the safe and effective operation of their FBCs by employing computational approaches yielding the following benefits to combat agglomeration in FBCs [21]:

1. Lower operating expenses: Computational approaches can help to lower operating costs by minimizing the requirement for trial-and-error testing, ultimately leading to fewer unplanned outages.

2. Increased safety: By identifying potential dangers and implementing mitigation mechanisms, computational tools can assist to increase the safety of an FBC.

3. Improved efficiency: By optimizing the operating conditions, computational approaches can help to improve the efficiency of an FBC.

In general, computational approaches are a useful tool for informing FBC operators. Operators can contribute to assure the safe, efficient, and cost-effective functioning of their FBCs by employing these approaches [22].

In such a scenario, numerical simulations are a useful tool for understanding the phenomena of agglomeration in fluidized beds [23] which may lead to adoption of preventative measures. In this study a unique approach is developed for the timely detection of the onset agglomeration by combining CFD with a population balance model for studying agglomeration formation [24]. There are numerous approaches for the onset of agglomeration, tracking the temperature, acoustic signals, or pressure in the reactor [25]. Bartels et al. [6] and Van Ommen et al. [26] presented extensive reviews related to detection of agglomeration due to the high temperatures and pressure fluctuations experimentally. The variation of experimental data can be observed after comparing these to the measurement when bed is fully fluidised. In actual tests, the detections are slightly delayed as the changes are not observable until major increase in temperature or drop in pressure has taken place. Current developments are focused to develop predictive tools or models to recognise agglomeration before de-fluidisation occurs. In continuation to the ongoing research, analysing pressure

fluctuations to detect agglomeration processes in fluidized beds is still practically a potential strategy [27]. The current paper describes a strategy for detecting agglomeration prior leading to total defluidization of the bed with the help of CFD techniques that are being tested and compared with the well-established experimental results (emissions, temperatures, and pressure profiles).

2. Biomass combustion in FBC

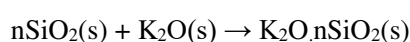
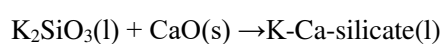
Biomass combustion is a complex process that involves a variety of chemical reactions. The exact reactions that occur will vary depending on the type of biomass, the operating conditions, and the presence of other substances [28]. Controlling the temperature, oxygen content, and the presence of catalysts can reduce the generation of nitrogen oxides and sulphur dioxide. The volatiles in biomass are made up of various organic components, for example hydrocarbons, oxygenated compounds, and nitrogenous chemicals. These volatiles are typically burned in two stages:

1. Primary combustion: In a fast, exothermic reaction, the volatiles are initially combusted. This reaction generates carbon monoxide, carbon dioxide, water vapour, and other combustion products.

2. Secondary combustion: In a slower, more regulated reaction, the carbon monoxide and other fuel-rich components in the combustion products are combusted. This process generates more carbon dioxide and water vapour.

Table 1 summarises the list of chemical reactions simulated in this research. Biomass combustion processes are frequently nonlinear, which implies that the rate of reaction is not simply proportional to the concentration of the reactants. This can make precise modelling of the reactions difficult [29]. The complexity of biomass combustion reactions makes accurate modelling difficult using typical computer approaches. New computational approaches that account for the nonlinearity and sensitivity of the reactions are required [30]. In this study, a high-performance computer (HPC) is used, and the results are validated using experimental data.

Agglomeration is a problem that can occur during the combustion of biomass in fluidized bed boilers. Agglomeration is the process of particles sticking together to form larger particles [31]. One of the major agglomeration processes that can occur in fluidized bed combustors are alkali-silicates reactions [32]. The silica in the bed material combines with the alkali metals in the biomass ash to generate low-melting alkali silicates in these processes. The alkali silicates can then cluster together to create bigger particles [33]. The alkali-silicates reactions are considered in this study for better understanding of agglomeration in fluidized bed reactors [34].



3. Experimental fluidized bed combustor

The system used in this work is a pilot plant of FBC installed at Beighton, Sheffield UK operated at a thermal rating of 65 kW_{th} with a heat exchanger and a cyclone separator to collect ash produced during combustion. The bed was initially heated during testing to 700 °C by utilization of the natural gas burners. Because of the heating of a bed and the incoming air, the bed became fluidized. Then, time was given to reach a steady state. The static bed height of 24 cm was used in all experiments. The height of combustor chamber is 4.75 meters and biomass inlet diameter are 0.02 meters with an outlet diameter of 0.60 meters. Seven thermocouples are installed at different positions to retrieve the bed temperature. The overview of pilot plant FBC at the University of Sheffield is shown in Fig. 1. Error! Reference source not found.

4. Model description and modeling equations

TFM and DEM are distinct CFD methods for simulating fluid and particle flow. The TFM is a macroscopic model that treats the fluid and the particles as two separate continua. The fluid is represented by a set of equations that describe its flow, and the particles are represented by a set of equations that describe their motion [36]. The TFM is a relatively simple model, but it can be used to simulate a wide range of fluid-particle flows [37].

DEM is a microscopic model treating particles individually. Interactions involve force laws among particles and drag/lift forces with the fluid [38]. Table 2 that summarizes the key differences between the TFM and the DEM [39].

In general, the TFM is a good choice for simulating large systems with many particles. In this research work population balance model (PBM) is used in conjunction with TFM because it can provide the detailed information that is needed to understand the behaviour of particles. The PBM can be used to predict the evolution of the particle size distribution, which is important for understanding the long-term behaviour of fluid-particle flows. The combination of the two models can provide more accurate results, a better understanding of the system.

By combining the TFM and the PBM, we can get more accurate predictions of the evolution of the particle size distribution. The discrete model of the PBM is used in this research work because it can be used to simulate systems with a large number of particles [40]. This is not possible with the continuous model of the PBM, which is only valid for systems with a small number of particles [41]. The discrete model of the PBM is a powerful tool for understanding and predicting the behaviour of systems with many particles. It is a valuable tool for researchers and engineers who are working on systems such as fluidized beds, crystallizers, and spray dryers [42].

Species transport model (STM) is adopted in this study to simulate biomass combustion reactions because it can be used to predict the distribution of different chemical species in the combustion chamber. This information can be used to optimize the combustion process and to reduce emissions. Eddy dissipation model of STM is a relatively simple model, but it is often used because it is relatively accurate and computationally efficient. The model has been used to simulate a wide variety of turbulent combustion systems, including flames, boilers, and engines. The significance of the EDM is that it provides a way to predict the rate of reaction in turbulent flows without having to know the details of the chemical kinetics [43]. This is important because the chemical kinetics of many combustion systems are complex and difficult to model. The EDM has been used to simulate a wide variety of turbulent combustion systems, and it has been shown to be a valuable tool for the design and optimization of these systems. Because the EDM model over predicts the temperature and is particularly valuable for design, the finite rate chemistry model (FRCM) is also employed to precisely predict the temperature profile in the combustor chamber [44].

The governing equations and their constitutive relations are mentioned in

Table 3.

The source term S represent the mass exchange between phases due to heterogeneous reactions in equation (3-1). In this study, we operated under the assumption that particle breakage did not take place; instead, particles underwent collisions to create agglomerates. Consequently, $B_{br,i}$ and $D_{br,i}$ were excluded from the Particle Balance (PB) equation (3-18). The two aggregation terms are delineated in equations (3-22) and (3-23), wherein particles of volume $(V-V')$ aggregate with particles of volume V' to generate particles with a combined volume V .

5. Simulation setup

The commercial CFD software package, ANSYS Fluent is used for the computational studies of agglomeration in FBCs. The experimental setup is adapted from the work of Morris et al. [35]. The geometry of the system in all dimensions is represented in Fig 2. The FBC has a height of 4.75 metres, and its air and biomass inlet diameters are 0.39 metres and 0.02 metres, respectively. The constructed numerical grid is made up of 60200 hexahedral elements that provide the best accuracy for a fixed number of cells with a $\frac{d_{cell}}{d_p}$ ratio of 10.

5.1 Phases materials, properties and boundary conditions

The phases and their important properties present in this simulation are given in

Table 4.

The composition of biomass (wheat straw) used in this simulation is given in

Table 5.

5.2 Closure models and restitution coefficients

Closure models and restitution coefficients are tabulated in

Table 6.

5.3 Discretization scheme

The velocity-pressure coupling is handled using the SIMPLE algorithm, which is phase-coupled. Finally, when considering the influence of viscosity, the $k-\epsilon$ viscous model implements the effect of turbulence. The spatial discretization is performed using the Quadratic Upstream Interpolation for Convective Kinematics (QUICK) scheme, which is commonly employed in this type of simulation to determine momentum and volume fraction. The overall discretization strategy is listed in Table 7.

5.4 Coupling technique

The convergence of a hydrodynamic and reaction model is a difficult task that has not been fully investigated by the scientific community. This is because the two models are coupled, meaning that they interact with each other. This can make it difficult to solve the equations for both models simultaneously. Therefore, the simulation order is very important, and that the communication between all the model equations played a key role in convergence. A step-by-step procedure is necessary to converge each model equation to reach the final and better solution of the system. This is an important contribution to the field of fluidized bed combustion modeling. It provides valuable insights into the challenges of convergence in these models, and it offers a step-by-step procedure for achieving convergence. This procedure can be used by other researchers to improve the accuracy of their fluidized bed combustion models. An overall coupling strategy is shown in Fig. 3.

6. Results and discussions

This study is a combination of hydrodynamics and chemical reactions with PBM. Primarily, the findings on the hydrodynamics are discussed as under:

6.1. Sand bed volume fraction

Fig. 4 displays snapshots of a 2D contour plot of the solid volume fraction taken at various flow times to demonstrate the behaviour of a fluidized bed. The red colour denotes the maximum particle volume fraction while blue colour indicates the minimum value of zero. Air bubbles generate at the base of chamber and move upward with the increasing size of bubble. Due to the extensive breaking and coalescence, the shape of the bubbles does not remain spherical. When the solid particles reach the bed surface, they are pushed against the wall by the burst of large bubbles. Then, because of gravity, the particles descend along the walls. These contours and field observational data through site viewing ports signifies inherent mixing and recirculation zones within the sand bed.

6.2 Agglomerate size distribution

Fig. 5(a) represents the initial particle size of quartz sand and Fig. 5(b) shows the agglomerates retrieved from the bottom of the bed after the defluidization time is detected. Largest agglomerate formed is forty times more than that of initial particle size. Pellet shaped agglomerates are formed specially with wheat straw when used as fuel. Some are solid sand structures while others are hollow and contain non-combusted char core [51], an indicative feature attributed to the high sodium and potassium containing fuels following melt-induced agglomeration mechanisms as observed in the case of wheat straw [51].

Clusters are formed in the system due to the collisions between the particles, PBM is used to determine the cluster size distribution in the system. The cluster formation is not very significant because chemical reactions trigger the agglomeration effect due to ash present in the biomass. But for the hydrodynamic study the particle size distribution can be seen from the Fig. 6. Diameters are normalized with the initial particle size, and it can be clearly seen that no significant clusters are present which disturb the U_{mf} and when the average particle size is calculated using the histogram of particle size distribution. It is found to be 3 times to that of initial particle size, which means only three particles grouped together and formed cluster. But from the experimental observations the particle size should be large enough so that U_{mf} requirement should be disturbed so significantly that the bed should not remain fluidized. So, from the above discussion it is revealed that clusters formed without chemical reactions but not large enough to defluidized the bed.

When the simulations are performed by coupling of all the models including chemical reactions and simulations continued at the detection of fluidization then the bell-shaped or normal particle size distribution is obtained a shown in Fig. 7. This curve can be divided into three groups i.e., primary particles, tightly packed particles, loosely packed particles. Primary particles cannot be divided into smaller particles. They typically make up only a small percentage or more precisely only 9% of the whole bed and 91% of the bed consists of loosely and tightly packed agglomerates that are held together by van der Waals forces or other attractive forces.

6.3 Temperature Profile of Fluidized Bed Combustor

Fig. 8. illustrates the temperature profile along the height of the combustor chamber. Species transport model is used to initiate the combustion reactions and both eddy dissipation and finite chemistry model is simulated and compared with the experimental results. It is found that when eddy dissipation model is used to simulate the combustion reactions; the bottom of the combustion chamber matches with the experimental results, however, it over predicts the temperature by 25-50 °C along the axial direction when compared to the experimental results because eddy dissipation model removes the influence of the chemical interactions and is generally acceptable for fast reacting fuels. When the system is simulated using the finite rate chemistry in which reactions kinetics are considered then a good comparison between simulated and experimental results is observed. BFBs usually operates in a temperature range of around 800-950 °C with lower temperatures in the dense bed region and this trend is generally seen in commercial scale operations.

Simulation results shows higher temperatures in the dense region which indicates better mixing and therefore uniformity of temperature. A sudden hike in temperature is seen above the dense region (i.e. 35 cm) liable due to the faster combustion reactions attributed to the burning of high volatile contents.

6.4 Emissions

Fig. 9 shows the CO₂ and pollutants emissions at the 6 vol.% O₂ standard reference. Biomass fuel (wheat straw) contains 0.9 wt.% Nitrogen contents which is the main reason for the formation of fuel NO_x. In fluidized bed combustion technology temperatures are generally lower than the temperatures (around 1300 °C) where thermal NO_x mechanisms become operational and contribute to the green houses gases and pollute the environment. The European Union Industrial Emissions Directive (EUIED) specifies 300mg/m³ to 200mg/m³ as the NO_x emission limit for big biomass combustion plants with a capacity of 50MW to 300MW. In this specific study the NO_x control is not the main objective hence the values are relatively higher than the commercial scale permissible limits, nevertheless the air staging commercial configurational changes have proven to reduce the emissions closer to said targets. In our case only primary air is introduced and simulated using the eddy dissipation sub model of species transport model, so higher is the CO formation and less CO₂ conversion in the free board region. The experimental work also lacks air-staging, only secondary air is introduced to avoid CO formation. In simulations only primary air is used which is the main reason of less CO conversion to CO₂. A biomass with low bound nitrogen content can be used to avoid NO_x formation as well. Literature [51] recommends the use of white wood as a fuel because it has low N₂ contents generally in the range of 0.1-0.2 wt.%.

6.5 Defluidization time

Fig. 10. shows experimental evolution of differential pressure across the sand bed in case of wheat straw as a biomass fuel. The experimental result shows a defluidization time of about 22 min. When the whole process is simulated using the devised coupling strategy of Eulerian based reactive CFD modeling with PBM it gives a defluidization time of 23 min and 27 s as shown in

Fig. 11. This simulation uses a high-performance computer (HPC) with 40 cores. Then the solution has stabilized around 2 min, there are oscillations around an average of 1000 Pa caused by the motion of the fluidized bed for nearly 18 min, indicating that no agglomeration has formed. After 18 min, the amplitude of the oscillations has significantly decreased, and the bed has begun to defluidize with formation of fluidizing air flow channels through the body of the bed. There is a sharp decrease in differential pressure at 23 min and 27 s, indicating the defluidization of the bed followed by a decreasing trend. This is due to the formation and accumulation of CaSiO_3 based agglomerates, in the chamber, which increased the average particle size. Nevertheless, the solid phases in the 750-850 °C range can equally comprise of calcium magnesium and sodium calcium silicates with a mixture of other minor phases such as sulphates and potassium silicates [54].

6.6 Agglomerates position

The radial profile of agglomerate mean volume fraction at three different axial locations is shown in Fig. 12. The volume fraction of agglomerates is higher near the walls and at the center of the rig, indicating the position of agglomerates.

The radial profile of the air mean volume fraction is depicted in Fig. 13. The air volume fraction is lower near the walls and at the centre of the rig, indicating that there is some strong hindrance that does not allow the air to pass through and, as a result, indicates the presence of agglomerates because the air does not overcome the adhesive forces between agglomerate particles and is no longer fluidizing the particles. The agglomerate samples retrieved from the defluidized bed, though not a direct measure, were found to be concentrated in the mid vertical and wall zonal strata as well.

7. Conclusion

In this research work, a CFD analysis of biomass combustion was performed, and the approach established for modeling combustion and agglomeration in a FBC has been outlined. The use of the population balance model (PBM) in conjunction with the Two-fluid model (TFM) for early prediction of agglomeration is adopted and the results are compared with the available experimental data. It is found that the use of PBM and TFM for early prediction of agglomeration is a promising approach and appropriate preventive measures can be initiated prior complete collapse of fluidizing bed. The findings of this study are important for the development of more efficient and sustainable biomass combustion technologies especially when the adopted strategies are implemented in large-scale industrial setups. Therefore, with continued

research, it is likely that these models will become more accurate and reliable, and they will be able to play an important role in the design and operation of biomass combustion systems.

Acknowledgements

The author acknowledges the fellowship received from the Pakistan Institute of Engineering and Applied Sciences. The authors acknowledge the Computational and Internet Services Division for providing the computational resources and are also grateful to Dr. Adnan Hamid, Dr. Kashif Rasheed and Dr. Muhammad Nadeem for their technical support and interactive discussions. The authors acknowledge UK EPSRC funding support through research grant No. EP/M01536X/1.

Declaration of interest

The authors declared no conflict of interest.

References

- [1] E. Ghiasi, "Bed Agglomeration Behavior in a Bubbling Fluidized-Bed Combustor," *Electronic Thesis and Dissertation Repository.*, vol. 3758, 2016, [Online]. Available: <https://ir.lib.uwo.ca/etdhttps://ir.lib.uwo.ca/etd/3758>
- [2] M. Bartels et al., "Agglomeration in fluidized beds at high temperatures: Mechanisms, detection and prevention," *Prog Energy Combust Sci*, vol. 34, no. 5, pp. 633–666, Oct. 2008, doi: 10.1016/J.PECS.2008.04.002.
- [3] A. Gungor and N. Eskin, "Two-dimensional coal combustion modeling of CFB," *International Journal of Thermal Sciences*, vol. 47, no. 2, pp. 157–174, Feb. 2008, doi: 10.1016/j.ijthermalsci.2007.01.017.
- [4] L. E. Fryda et al., "Agglomeration in fluidised bed gasification of biomass," *Powder Technol*, vol. 181, no. 3, pp. 307–320, Feb. 2008, doi: 10.1016/j.powtec.2007.05.022.
- [5] Y. Niu et al., "Ash-related issues during biomass combustion: Alkali-induced slagging, silicate melt-induced slagging (ash fusion), agglomeration, corrosion, ash utilization, and related countermeasures," *Prog Energy Combust Sci*, vol. 52, pp. 1–61, Feb. 2016, doi: 10.1016/j.pecs.2015.09.003.
- [6] M. Bartels et al., "Agglomeration in fluidized beds at high temperatures: Mechanisms, detection and prevention," *Prog Energy Combust Sci*, vol. 34, no. 5, pp. 633–666, Oct. 2008, doi: 10.1016/j.pecs.2008.04.002.

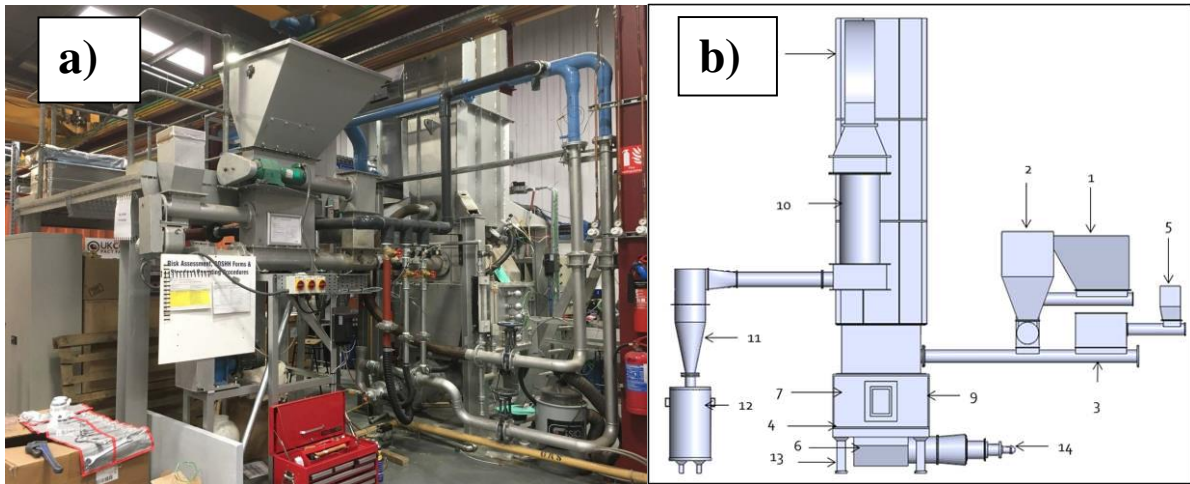
- [7] M. Öhman et al., “Bed agglomeration characteristics and mechanisms during gasification and combustion of biomass fuels,” *Energy and Fuels*, vol. 19, no. 4, pp. 1742–1748, Jul. 2005, doi: 10.1021/EF040093W.
- [8] J. Nisamaneenate et al., “Mitigating bed agglomeration in a fluidized bed gasifier operating on rice straw,” *Energy Reports*, vol. 6, pp. 275–285, Nov. 2020, doi: 10.1016/j.egy.2020.08.050.
- [9] E. Ghiasi et al., “Bed Agglomeration Behavior in a Bubbling Fluidized-Bed Bed Agglomeration Behavior in a Bubbling Fluidized-Bed Combustor Combustor,” 2016. [Online]. Available: <https://ir.lib.uwo.ca/etdhttps://ir.lib.uwo.ca/etd/3758>
- [10] F. Scala et al., “Characterization and early detection of bed agglomeration during the fluidized bed combustion of olive husk,” *Energy and Fuels*, vol. 20, no. 1, pp. 120–132, Jan. 2006, doi: 10.1021/EF050236U.
- [11] C. Yu et al., “Experimental determination of agglomeration tendency in fluidized bed combustion of biomass by measuring slip resistance,” *Fuel*, vol. 128, pp. 14–20, Jul. 2014, doi: 10.1016/j.fuel.2014.03.002.
- [12] P. Chaivatamaset et al., “Bed Particle Agglomeration and Defluidization in the Rubber Wood and Coir-Fired Fluidized Bed,” *Waste Biomass Valorization*, vol. 10, no. 11, pp. 3457–3470, Nov. 2019, doi: 10.1007/S12649-018-0358-Y.
- [13] P. Lahijani et al., “Gasification of palm empty fruit bunch in a bubbling fluidized bed: A performance and agglomeration study,” *Bioresour Technol*, vol. 102, no. 2, pp. 2068–2076, Jan. 2011, doi: 10.1016/j.biortech.2010.09.101.
- [14] X. Xin et al., “Insights into Preventing Fluidized Bed Material Agglomeration in Fast Pyrolysis of Acid-Leached Pine Wood,” *Energy and Fuels*, vol. 33, no. 5, pp. 4254–4263, May 2019, doi: 10.1021/ACS.ENERGYFUELS.8B04178.
- [15] E. Natarajan et al., “Experimental determination of bed agglomeration tendencies of some common agricultural residues in fluidized bed combustion and gasification,” *Biomass Bioenergy*, vol. 15, no. 2, pp. 163–169, Aug. 1998, doi: 10.1016/S0961-9534(98)00015-4.
- [16] R. Chirone et al., “Mechanism and prediction of bed agglomeration during fluidized bed combustion of a biomass fuel: Effect of the reactor scale,” *Chemical Engineering Journal*, vol. 123, no. 3, pp. 71–80, Oct. 2006, doi: 10.1016/j.cej.2006.07.004.
- [17] W. Zhou et al., “Two-dimensional computational fluid dynamics simulation of coal combustion in a circulating fluidized bed combustor,” *Chemical Engineering Journal*, vol. 166, no. 1, pp. 306–314, Jan. 2011, doi: 10.1016/j.cej.2010.09.048.

- [18] S. Banerjee et al., “An Eulerian Approach to Computational Fluid Dynamics Simulation of a Chemical-Looping Combustion Reactor With Chemical Reactions,” *Journal of Energy Resources Technology, Transactions of the ASME*, vol. 138, no. 4, pp. 1–9, 2016, doi: 10.1115/1.4031968.
- [19] R. F. Nascimento et al., “Agglomeration in fluidized bed: Bibliometric analysis, a review, and future perspectives,” *Powder Technology*, vol. 406. Elsevier B.V., Jul. 01, 2022. doi: 10.1016/j.powtec.2022.117597.
- [20] M. Bartels et al., “Detecting and counteracting agglomeration in fluidized bed biomass combustion,” *Energy and Fuels*, vol. 23, no. 1, pp. 157–169, Jan. 2009, doi: 10.1021/EF8005788.
- [21] S. Oka et al., “Fluidized Bed Combustion,” 2004.
- [22] M. Bartels et al., “Detection of agglomeration and gradual particle size changes in circulating fluidized beds,” *Powder Technol*, vol. 202, no. 1–3, pp. 24–38, Aug. 2010, doi: 10.1016/j.powtec.2010.03.035.
- [23] S. Leimbach et al., “Early Detection of Agglomeration in Fluidized Beds by Means of Frequency Analysis of Pressure Fluctuations,” *Energy and Fuels*, vol. 36, no. 9, pp. 4924–4932, May 2022, doi: 10.1021/acs.energyfuels.1c04356.
- [24] D. Ramkrishna et al., “Population balance modeling: Current status and future prospects,” *Annu Rev Chem Biomol Eng*, vol. 5, pp. 123–146, 2014, doi: 10.1146/annurev-chembioeng-060713-040241.
- [25] J. Nijenhuis et al., “A method for agglomeration detection and control in full-scale biomass fired fluidized beds,” *Chem Eng Sci*, vol. 62, no. 1–2, pp. 644–654, Jan. 2007, doi: 10.1016/j.ces.2006.09.041.
- [26] J. R. Van Ommen et al., “Time-series analysis of pressure fluctuations in gas–solid fluidized beds – A review,” *International Journal of Multiphase Flow*, vol. 37, no. 5, pp. 403–428, Jun. 2011, doi: 10.1016/J.IJMULTIPHASEFLOW.2010.12.007.
- [27] M. Punčochář et al., “Origin of pressure fluctuations in fluidized beds,” *Chem Eng Sci*, vol. 60, no. 5, pp. 1193–1197, Mar. 2005, doi: 10.1016/j.ces.2004.09.054.
- [28] A. A. Khan et al., “Biomass combustion in fluidized bed boilers: Potential problems and remedies,” *Fuel Processing Technology*, vol. 90, no. 1, pp. 21–50, Jan. 2009, doi: 10.1016/J.FUPROC.2008.07.012.
- [29] L. Ma, J. M. Jones et al., “Modelling the combustion of pulverized biomass in an industrial combustion test furnace,” *Fuel*, vol. 86, no. 12–13, pp. 1959–1965, Aug. 2007, doi: 10.1016/J.FUEL.2006.12.019.

- [30] S. Zahirovic et al., “Advanced CFD modelling of pulverised biomass combustion,” *Proceedings of the 6th International conference in science in thermal and chemical biomass conversion*, 2004.
- [31] G. A. Ryabov et al., “Agglomeration during Fluidized Bed Combustion and Gasification of Fuels,” *Thermal Engineering*, vol. 66, no. 9, pp. 635–651, Sep. 2019, doi: 10.1134/S0040601519090040.
- [32] A. B. Khadilkar et al., “Integrated modeling methodology for ash agglomeration in poly-disperse fluidized beds using particle population framework,” *Powder Technol*, vol. 384, pp. 368–378, May 2021, doi: 10.1016/j.powtec.2021.01.073.
- [33] S. V. Vassilev et al., “Ash contents and ash-forming elements of biomass and their significance for solid biofuel combustion,” *Fuel*, vol. 208, pp. 377–409, 2017, doi: 10.1016/j.fuel.2017.07.036.
- [34] J. D. Morris et al., “Mechanisms and mitigation of agglomeration during fluidized bed combustion of biomass: A review,” *Fuel*, vol. 230, pp. 452–473, Oct. 2018, doi: 10.1016/J.FUEL.2018.04.098.
- [35] J. D. Morris et al., “Agglomeration and the effect of process conditions on fluidized bed combustion of biomasses with olivine and silica sand as bed materials: Pilot-scale investigation,” *Biomass Bioenergy*, vol. 142, no. August, p. 105806, 2020, doi: 10.1016/j.biombioe.2020.105806.
- [36] V. Chauhan et al., “A transient Eulerian-Eulerian simulation of bubbling regime hydrodynamics of coal ash particles in fluidized bed using different drag models,” *Advanced Powder Technology*, vol. 33, no. 1, Jan. 2022, doi: 10.1016/j.apt.2021.12.004.
- [37] T. M. Ismail et al., “Eulerian - Eulerian CFD model on fluidized bed gasifier using coffee husks as fuel,” *Appl Therm Eng*, vol. 106, pp. 1391–1402, Aug. 2016, doi: 10.1016/j.applthermaleng.2016.06.102.
- [38] C. Gu *et al.*, “CFD-DEM simulation of distribution and agglomeration characteristics of bendable chain-like biomass particles in a fluidized bed reactor,” *Fuel*, vol. 340, p. 127570, May 2023, doi: 10.1016/j.fuel.2023.127570.
- [39] L. Fries et al., “DEM-CFD modeling of a fluidized bed spray granulator,” *Chem Eng Sci*, vol. 66, no. 11, pp. 2340–2355, 2011, doi: 10.1016/j.ces.2011.02.038.
- [40] M. Yang et al., “Numerical simulation on the effects of bubble size and internal structure on flow behavior in a DAF tank: A comparative study of CFD and CFD-PBM approach,” *Chemical Engineering Journal Advances*, vol. 7, Aug. 2021, doi: 10.1016/j.cej.2021.100131.
- [41] S. Ehrman, “Population balance modeling -an application in particle technology,” *Design*, 2005.

- [42] O. Maurstad, "Population Balance Modeling of Agglomeration in Granulation Processes," *Vasa*, pp. 1–108, 2002, [Online]. Available: <http://medcontent.metapress.com/index/A65RM03P4874243N.pdf>
- [43] M. Beneš *et al.*, "Numerical simulation of fluidization for application in oxyfuel combustion," *Discrete and Continuous Dynamical Systems - Series S*, vol. 14, no. 3, pp. 769–783, Mar. 2021, doi: 10.3934/dcdss.2020232.
- [44] T. D. Canonsburg, "ANSYS Fluent Theory Guide," *ANSYS Inc., USA*, vol. 15317, no. November, p. 814, 2013, [Online].
- [45] D. Gidaspow, *Multiphase Flow and Fluidization: Continuum and Kinetic Theory Descriptions*. 2012. doi: 10.1016/C2009-0-21244-X.
- [46] S. O. Brien *et al.*, "Study of Gas-Solid Fluidized Bed - Tuning STUDY OF GAS-SOLID FLUIDIZED BED - TUNING SYAMLAL O ' BRIEN," no. July, 2014.
- [47] D. G. Schaeffer, "Instability in the evolution equations describing incompressible granular flow," *J Differ Equ*, vol. 66, no. 1, pp. 19–50, 1987, doi: 10.1016/0022-0396(87)90038-6.
- [48] D. J. Gunn, "Transfer of heat or mass to particles in fixed and fluidised beds," *Int J Heat Mass Transf*, vol. 21, no. 4, pp. 467–476, Apr. 1978, doi: 10.1016/0017-9310(78)90080-7.
- [49] C. K. K. Lun *et al.*, "Kinetic theories for granular flow: Inelastic particles in Couette flow and slightly inelastic particles in a general flowfield," *J Fluid Mech*, vol. 140, no. March 1984, pp. 223–256, 1984, doi: 10.1017/S0022112084000586.
- [50] A. Aissa *et al.*, "Ranz and marshall correlations limits on heat flow between a sphere and its surrounding gas at high temperature," *Thermal Science*, vol. 19, no. 5, pp. 1521–1528, 2015, doi: 10.2298/TSCI120912090A.
- [51] Morris, J. (2021). Mechanisms and mitigation of agglomeration during fluidized bed combustion of biomass (Doctoral dissertation, University of Sheffield).

Figures:



- | | | | | |
|---------------------|-----------------------|--------------------------|-----------------------|--|
| 1. Big Hopper | 4. Distributor
Bed | 7. Combustion
Chamber | 10. Heat
Exchanger | 13. Base Support Structure |
| 2. Middle
Hopper | 5. Small
Hopper | 8. Free Board | 11. Cyclone | 14. Natural Gas Initial
Firing Burner |
| 3. Screw
Feeder | 6. Plenum | 9. Side wall Plugs | 12. Ash
Collector | |

Fig. 1. (a) Pilot scale fluidized bed biomass combustor adapted from the work of Morris et al. [35], (b) Solid works drawing of the testing facility.

[Cannot see 8 in the figure? Please check]

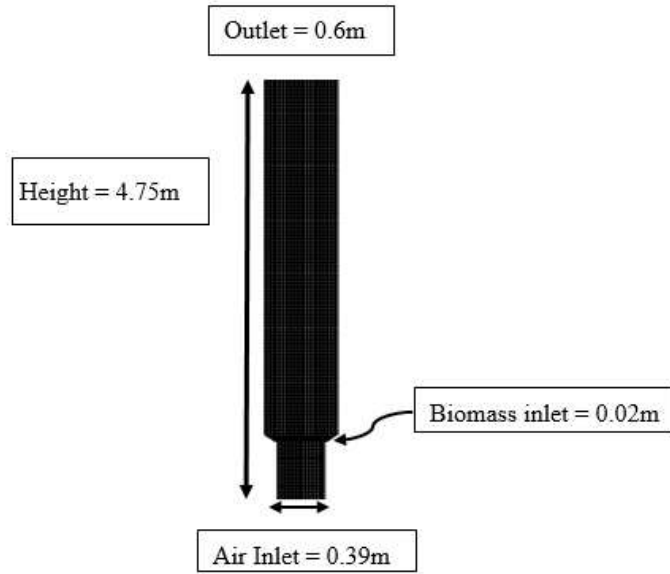


Fig. 2. Geometry of 65-kWth pilot scale FBC.

[Words in the figure are not very clear, please improve. Thanks]

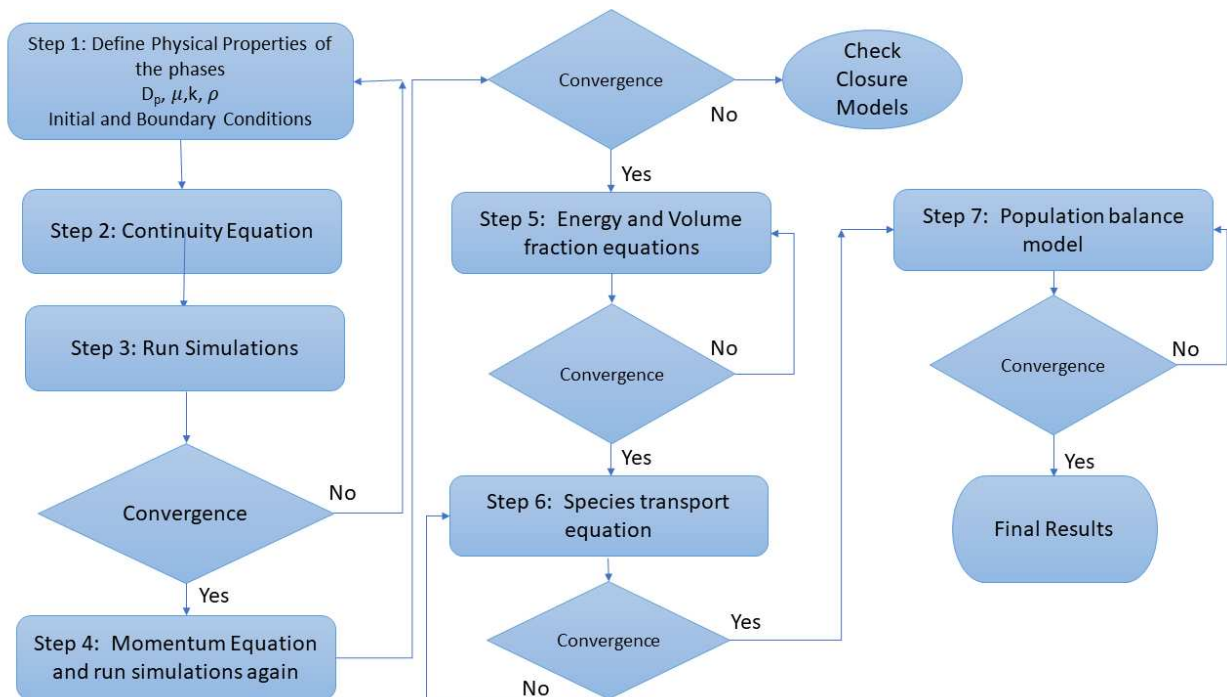


Fig. 3. Coupling scheme to converge models.

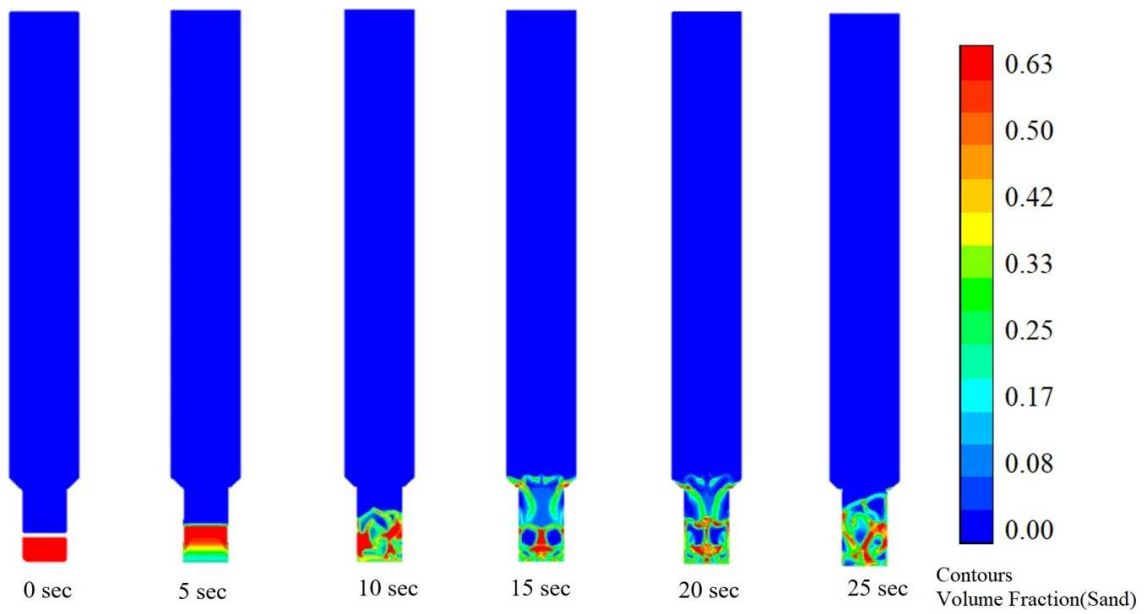


Fig. 4. Instantaneous contours of sand volume fraction.

[Please revise sec to be s] [(sand) please add a space before (), also for other figures, thanks.]



Fig. 5. (a) Sand bed particles (640 μm); (b) agglomerates of various sizes after defluidization.

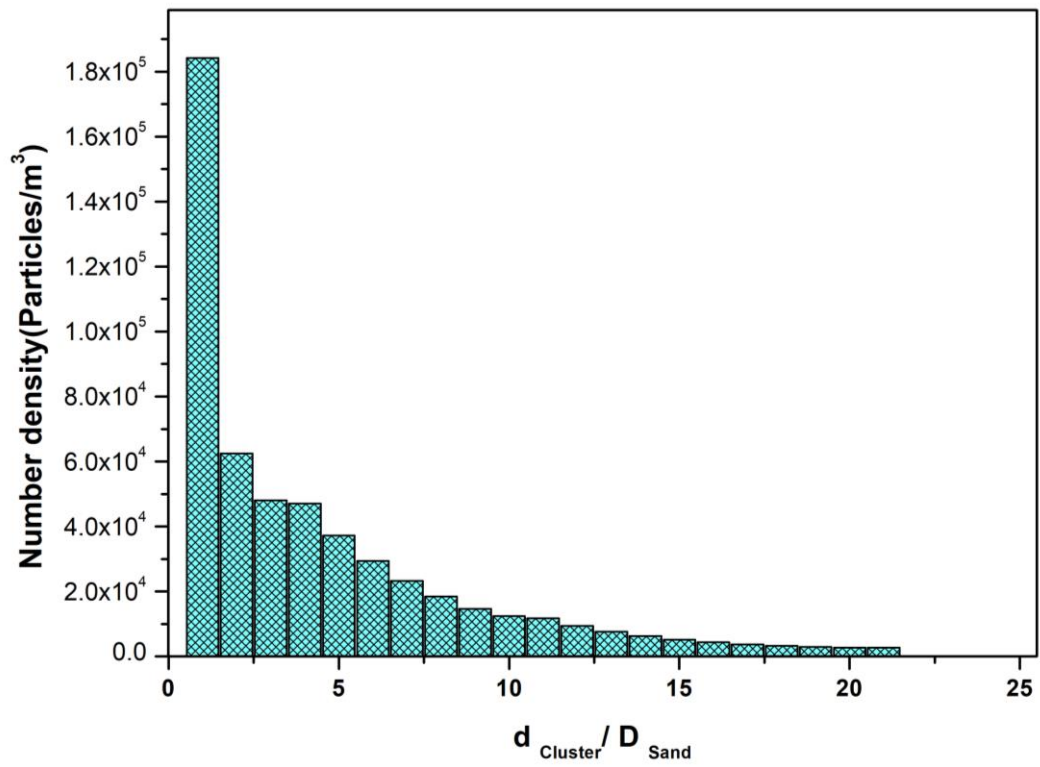


Fig. 6. Histogram of particle size distribution.

[On axis please add a space before (), also for other figures, thanks.]

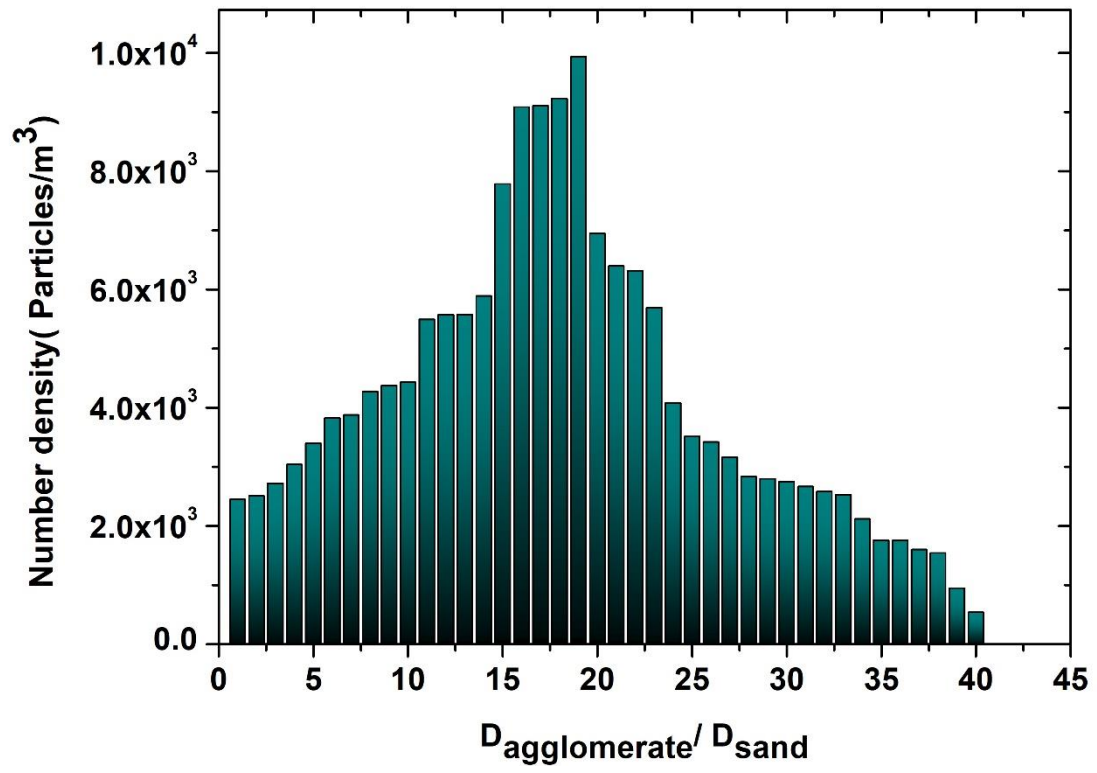


Fig. 7. Histogram of agglomerates size distribution in the rig.

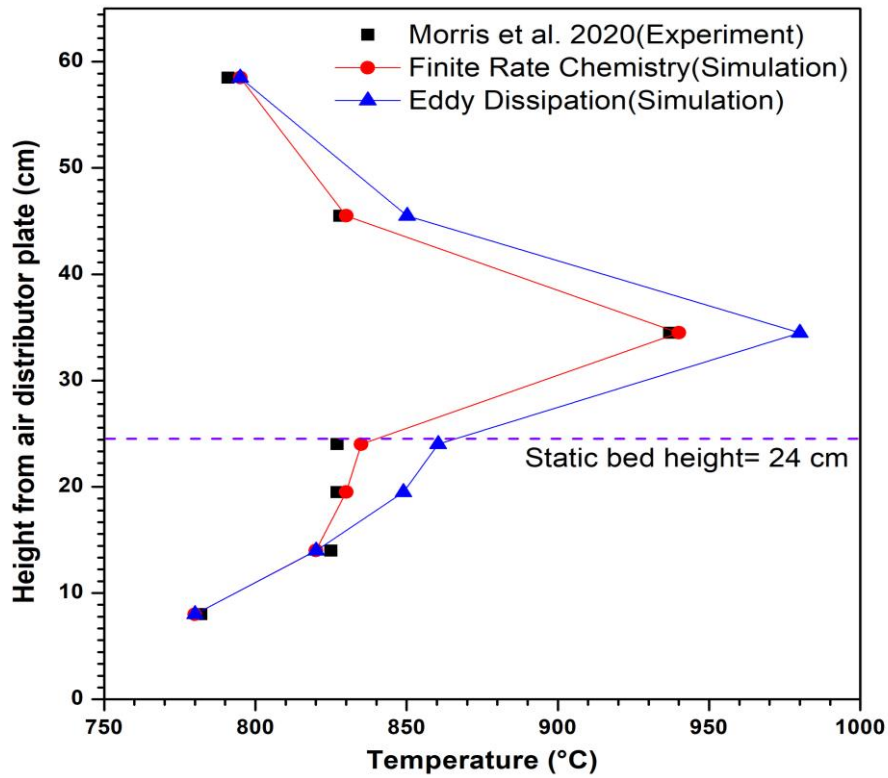


Fig. 8. Temperature profile along the height of combustor.

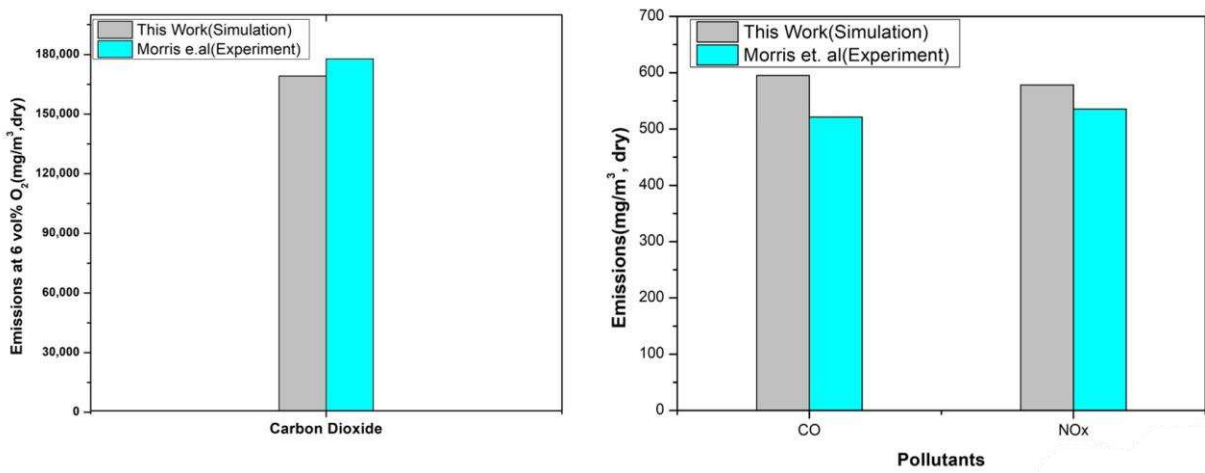


Fig. 9. Comparison of emissions between experimental and simulation results (using eddy dissipation model).

[In the figure, please add year for the 2 Morris et al, thanks]

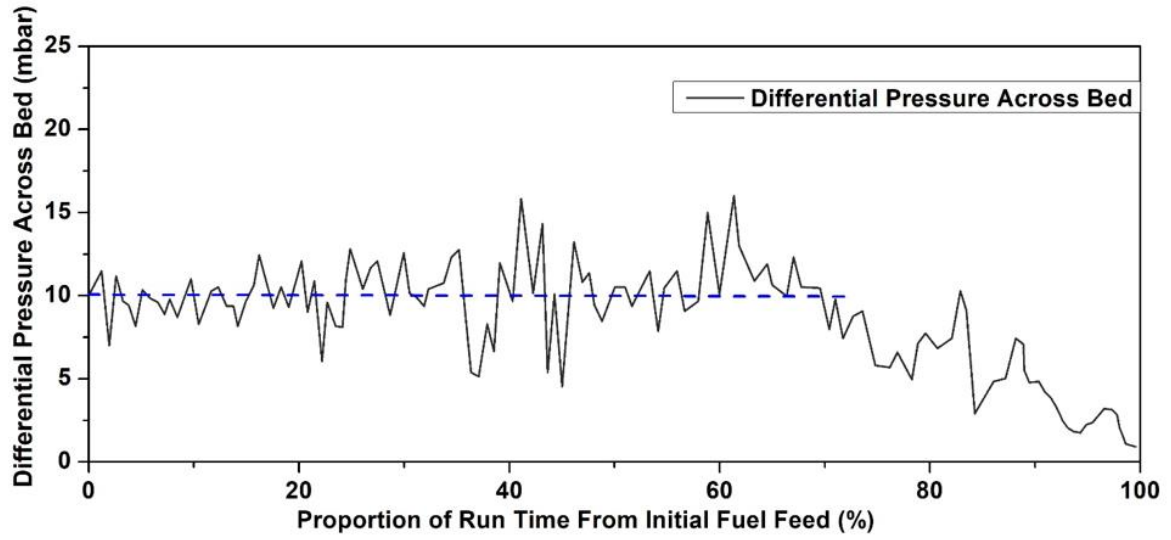


Fig. 10. Experimental Evolution of Differential Pressure across the sand bed. Adapted from the work of Morris et al. [54].

[On the axis, please only keep the 1st letter of 1st word in capital letter, please revise all these figures, thanks]

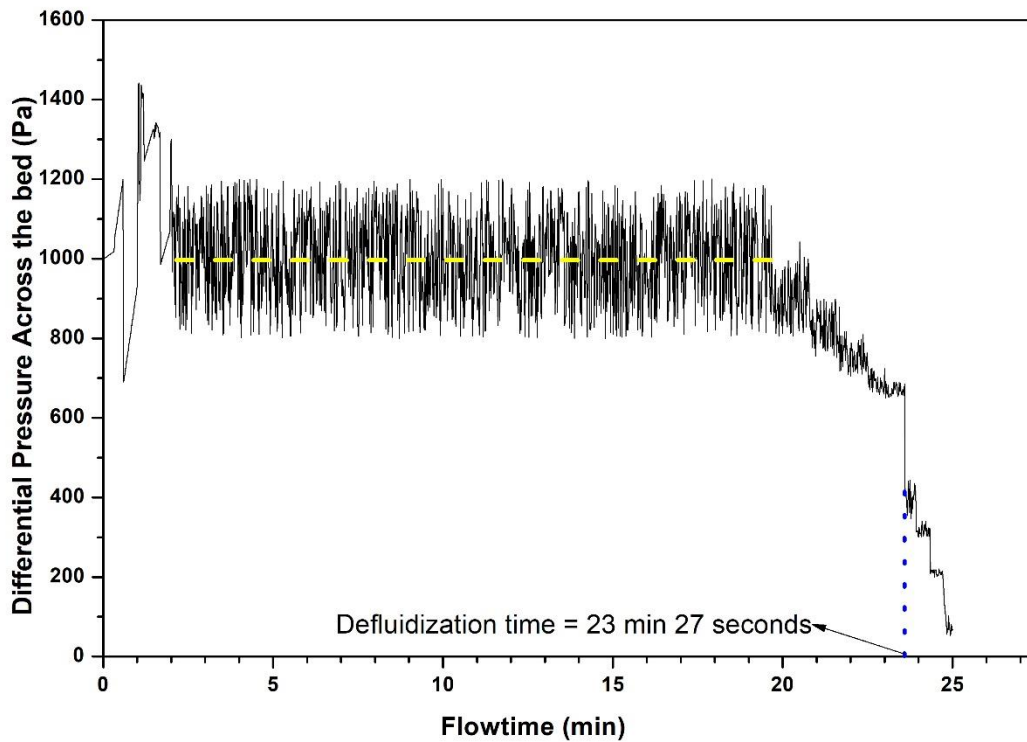


Fig. 11. Differential pressure fluctuations across the bed (Decline in DP corresponds to defluidization).

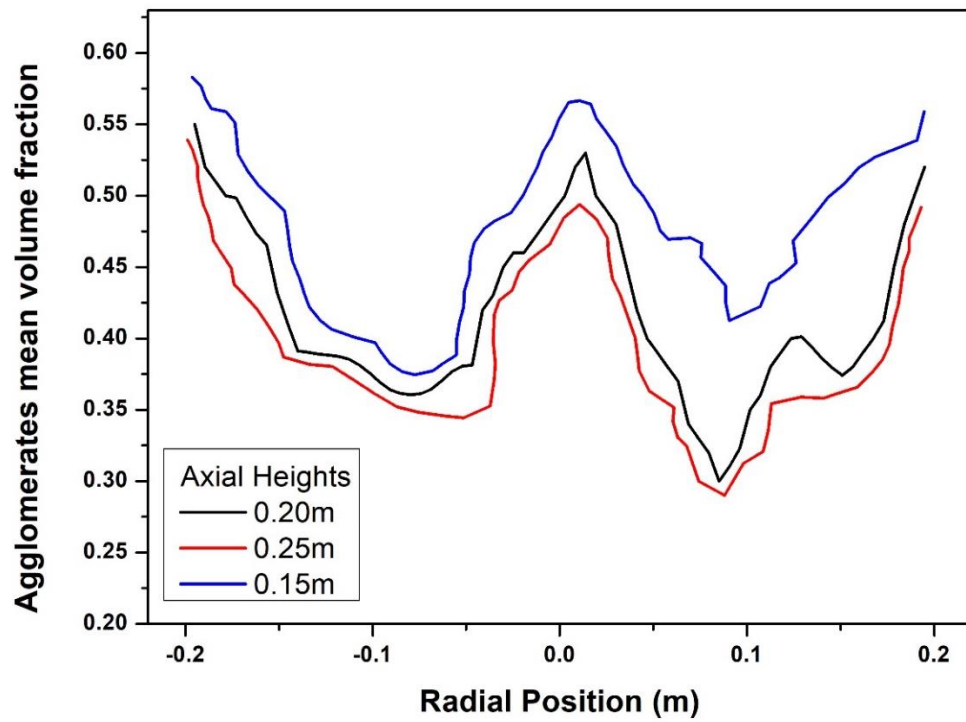


Fig. 12. Radial Profile of agglomerate mean volume fraction.

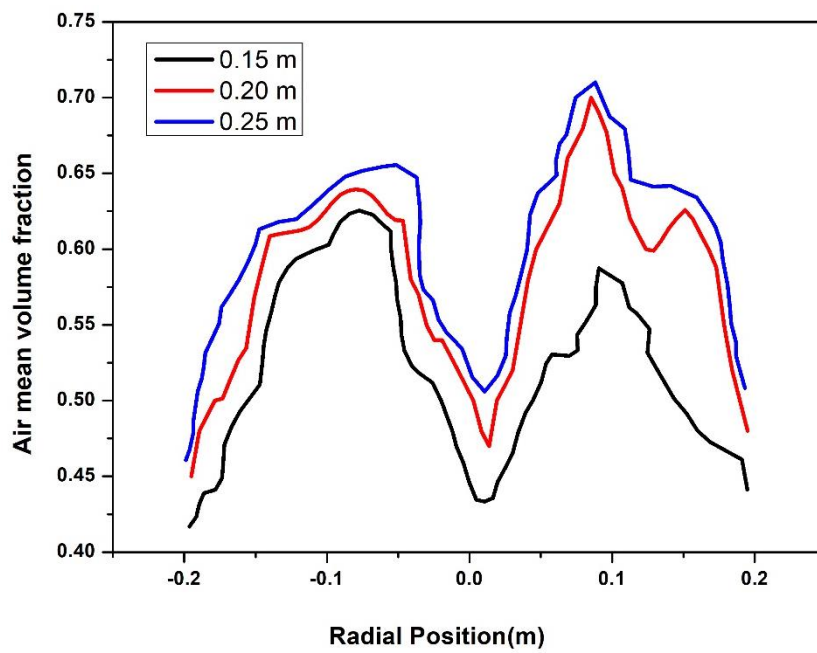


Fig. 13. Radial profile of air mean volume fraction.

Tables:

Table 1: List of chemical reactions.

Process	Reaction	Type	Temperature
Drying	$\text{H}_2\text{O}(\text{l}) \rightarrow \text{H}_2\text{O}(\text{g})$	Endothermic	Around 100 °C
Devolatilization	$\text{Volatiles} + \frac{3}{2}\text{O}_2 \rightarrow \text{CO}_2 + 2\text{H}_2\text{O}$	Exothermic	Around 500 °C
Char Burnout	$\text{C}(\text{s}) + \frac{1}{2}\text{O}_2 \rightarrow \text{CO}(\text{g})$	Exothermic	Above 700 °C
	$\text{CO}(\text{g}) + \frac{1}{2}\text{O}_2 \rightarrow \text{CO}_2(\text{g})$		
Nitrogen Reactions	$\text{N}_2 + \text{O}_2 \rightarrow 2\text{NO}$	Exothermic	Above 800 °C
Sulfur Reactions	$\text{S} + \text{O}_2 \rightarrow \text{SO}_2$	Exothermic	Above 800 °C

Table 2: Difference between TFM and DEM

Feature	Two-fluid model (TFM)	Discrete element method (DEM)
Accuracy	Less accurate	More accurate
Computational efficiency	More computationally efficient	Less computationally efficient
Application range	Large systems with many particles	Small systems with a small number of particles

Table 3: Governing equations for simulation

[The marked dots look lower, should be centered? Please check and revise.]

Equation Name	Expression	Eq. No.
Continuity Equation (k=s,g)	$\frac{\partial}{\partial t}(\varepsilon_k \rho_k) + \nabla \cdot (\varepsilon_k \rho_k \vec{v}_k) = S_k$	(3-1)
	$\varepsilon_s + \varepsilon_g = 1$	(3-2)
Momentum Equation (Gas phase)	$\frac{\partial}{\partial t}(\varepsilon_g \rho_g \vec{v}_g) + \nabla \cdot (\varepsilon_g \rho_g \vec{v}_g \vec{v}_g) = -\varepsilon_g \nabla P + \nabla \cdot \bar{\tau}_g + \varepsilon_g \rho_g \vec{g} + \vec{F}_{k,g}$	(3-3)
Gas Phase Stress	$\bar{\tau}_g = \mu_{1,g}(\nabla \vec{v}_g + \nabla \vec{v}_g^T) - \frac{2}{3} \mu_{1,g} \nabla \cdot \vec{v}_g$	(3-4)
Momentum Equation (Solid phase)	$\frac{\partial}{\partial t}(\varepsilon_s \rho_s \vec{v}_s) + \nabla \cdot (\varepsilon_s \rho_s \vec{v}_s \vec{v}_s) = -\varepsilon_s \nabla p - \nabla \cdot P_s + \nabla \cdot \bar{\tau}_s + \varepsilon_s \rho_s \vec{g} + \vec{F}_{k,s}$	(3-5)
Solid phase Shear viscosity	$\mu_s = \mu_{s,col} + \mu_{s,kin} + \mu_{s,fr}$	(3-6)
	$\mu_{s,col} = \frac{4}{5} \varepsilon_s \rho_s d_s g_{o,ss} (1 + e_{ss}) \left(\frac{\theta_s}{\pi}\right)^{\frac{1}{2}}$	(3-7)
	$\mu_{s,kin} = \frac{\varepsilon_s \rho_s d_s \sqrt{\theta_s \pi}}{6(3 - e_{ss})} \left[1 + \frac{2}{5} (1 + e_{ss})(3e_{ss} - 1) \varepsilon_s g_{o,ss} \right]$	(3-8)
	$\mu_{s,fr} = \frac{P_s \sin \phi}{2\sqrt{I_{2D}}}$	(3-9)
Solid stress tensor	$\bar{\tau}_s = \mu_s(\nabla \vec{v}_s + \nabla \vec{v}_s^T) + \left(\lambda_s - \frac{2}{3} \mu_{1,g}\right) \nabla \vec{v}_s$	(3-10)
Solid bulk viscosity	$\lambda_s = \frac{4}{3} \varepsilon_s \rho_s d_s g_{o,ss} (1 + e_{ss}) \left(\frac{\theta_s}{\pi}\right)^{\frac{1}{2}}$	(3-11)
Turbulence Model k-ε Equations (Mixture)	$\frac{\partial}{\partial t}(\rho k) + \frac{\partial}{\partial x_i}(\rho k u_i) = \frac{\partial}{\partial x_j} \left[\left(\mu + \frac{\mu_t}{\sigma_k} \right) \frac{\partial k}{\partial x_j} \right] + G_k + G_b - \rho \varepsilon - Y_M + S_k$	(3-12)
	$\frac{\partial}{\partial t}(\rho \varepsilon) + \frac{\partial}{\partial x_i}(\rho \varepsilon u_i) = \frac{\partial}{\partial x_j} \left[\left(\mu + \frac{\mu_t}{\sigma_\varepsilon} \right) \frac{\partial \varepsilon}{\partial x_j} \right] + C_{1\varepsilon} \frac{\varepsilon}{k} (G_k + C_{3\varepsilon} G_b) - C_{2\varepsilon} \rho \frac{\varepsilon^2}{k} + S_\varepsilon$	(3-13)
Energy Equation	$\frac{\partial}{\partial t}(\varepsilon_g \rho_g H_g) + \nabla \cdot (\varepsilon_g \rho_g u_g H_g) = \nabla \cdot (\alpha_g \nabla T_g) + Q_{gs} + S_{gs} H_s$	(3-14)
	$\frac{\partial}{\partial t}(\varepsilon_s \rho_s H_s) + \nabla \cdot (\varepsilon_s \rho_s u_s H_s) = \nabla \cdot (\alpha_s \nabla T_s) + Q_{sg} + S_{sg} H_s$	(3-15)
	$H = \sum_{i=1}^n Y_i H_i$	(3-16)

Species Equation	$\frac{\partial}{\partial t}(\varepsilon_g \rho_g Y_{g,i}) + \nabla \cdot (\varepsilon_g \rho_g u_g Y_{g,i}) = -\nabla \cdot \varepsilon_g J_{g,i} + \varepsilon_g R_{g,i} + R_{s,i}$	(3-17)
Population Balance Model Equation	$\frac{\partial}{\partial t}(\rho_s \varepsilon_i) + \nabla(\rho_s \mu_i \varepsilon_i) + \frac{\partial}{\partial V} \left(\frac{G_v \rho_s \varepsilon_i}{V} \right)$	(3-18)
	$= \rho_s V_i (B_{ag,i} - D_{ag,i} + B_{br,i} - D_{br,i}) + 0^i \rho_s V_0 \dot{n}_0$	
	$\varepsilon_i = N_i V_i \quad i = 0, 1, \dots, N$	(3-19)
	$N_i(t) = \int_{V_i}^{V_{i+1}} n(V, t) dV$	(3-20)
	$\frac{\partial}{\partial x} \left(\frac{G_v \rho_s \varepsilon_i}{V} \right) = \rho_s V_i \left[\left(\frac{G_{v,i-1} N_{i-1}}{V_i - V_{i-1}} \right) - \left(\frac{G_{v,i} N_i}{V_{i+1} - V_i} \right) \right]$	(3-21)
	$B_{ag} = \frac{1}{2} \int_0^V a(V - V', V') n(V - V') dV'$	(3-22)
	$D_{ag} = \int_0^\infty a(V, V') n(V) n(V') dV'$	(3-23)
Luo Aggregation Kernel	$\Omega_{ag}(V_i, V_j) = \omega_{ag}(V_i, V_j) P_{ag}(V_i, V_j)$	(3-24)
	$\omega_{ag}(V_i, V_j) = \frac{\pi}{4} (d_i + d_j)^2 n_i n_j \bar{u}_{ij}$	(3-25)
	$\bar{u}_{ij} = (\bar{u}_i^2 + \bar{u}_j^2)^{\frac{1}{2}}$	(3-26)
	$\bar{u}_i = 1.43(\varepsilon d_i)^{1/3}$	(3-27)
	$P_{ag} = \exp \left\{ -c_1 \frac{[0.75(1 + x_{ij}^2)(1 + x_{ij}^3)]^{\frac{1}{2}}}{\left(\frac{\rho_s}{\rho_g} + 0.5 \right)^{\frac{1}{2}} (1 + x_{ij})^3} We_{ij}^{\frac{1}{2}} \right\}$	(3-28)
	$We_{ij} = \frac{\rho_l d_i (\bar{u}_{ij})^2}{\sigma}$	(3-29)

Table 4 Phase properties and boundary conditions

Parameter	Sand	Fuel	Air
Particle/fluid density (kg m ⁻³)	2650	800	1.225
Particle diameter (μm)	640	5	-
Thermal conductivity (Wm ⁻¹ K ⁻¹)	0.21	0.20	0.024
Specific heat (J kg ⁻¹ K ⁻¹)	800	1336	1006
Molecular weight (kg kmol ⁻¹)	60.08	26.25	28.996
Viscosity (kg m ⁻¹ s ⁻¹)	-	-	1.8 × 10 ⁻⁵
Static bed height (m)	0.24	-	-
Sand phase composition	Mass fraction in percentage (%)		
SiO ₂	97.15		
Fe ₂ O ₃	1.96		
CaO	0.20		
KaO	0.69		
Boundary Conditions			
Air inlet		117.6 kg/h	
Biomass inlet		10.2 kg/h	
Outlet		Pressure outlet	
Wall		No slip	

Table 5 Composition of biomass (wheat straw).

Column title?	Column title?	Biomass composition (%)
Ultimate analysis (wt.%)	C	40.50
	H	4.80
	O	40.00
	N	0.90
	S	0.10
Proximate analysis (wt.%)	Moisture	7.12
	Volatiles	68.38
	Char	17.82
	Ash	6.67
	Biomass Formula	$C_{1.34}H_{1.11}N_{0.009}S_{0.001}O$
Column title?	Column title?	Mass fraction as % of total ash
Ash composition	SiO ₂	38.4
	K ₂ O	19.8
	P ₂ O ₅	4.8
	MgO	3.6
	CaO	21.1
	Al ₂ O ₃	1.6
	Na ₂ O	6.3
	Fe ₂ O ₃	1.0
	MnO	0.1
TiO ₂	0.3	

[Please revise the numbers to be subscript]

Table 6. Closure models

Solid phase (sand)		Gas phase (air)	
Granular temperature model	Algebraic	Density	1.225 kg/m ³
Granular viscosity	Gidaspow [45]	Viscosity	1.8×10 ⁻⁵ kg/m-s ??
Particle–particle restitution coefficient	0.9	Gas-solid drag law	Syamlal-Obrien [46]
Granular frictional viscosity	Schaeffer [47]	Gas-solid heat transfer coefficient	Gunn Model [48]
Granular bulk viscosity	Lun et al. [49]	Solid-solid heat transfer coefficient	Ranz-Marshal correlation [50]
Max. packing limit	0.63		

Table 7. Discretization Scheme

Equation	Scheme
Momentum	QUICK
Turbulent kinetic energy	1 st order upwind
Energy	2 nd order upwind
Volume Fraction	QUICK
Turbulent dissipation rate	2 nd order upwind
Sand Bin	2 nd order upwind
Physical time step size (s)	1 × 10 ⁻⁵
Time implicit formulation	1st order